Published in final edited form as:
Bone. 2010 June ; 46(6): 1564–1573. doi:10.1016/j.bone.2010.02.014.

Osteopontin Deficiency Increases Bone Fragility but Preserves Bone Mass

Philipp J. Thurner[1,2], **Carol G. Chen**[1], **Sophi Ionova-Martin**[3,4], **Luling Sun**[3,4], **Adam Harman**[5], **Alexandra Porter**[5], **Joel W. Ager III**[3], **Robert O. Ritchie**[3,4], and **Tamara Alliston**[1,6]

Philipp J. Thurner: p.thurner@soton.ac.uk; Carol G. Chen: carol.chen@ucsf.edu; Sophi Ionova-Martin: sophi@berkeley.edu; Luling Sun: llsun@berkeley.edu; Adam Harman: adam.harman05@imperial.ac.uk; Alexandra Porter: a.porter@imperial.ac.uk; Joel W. Ager: JWAger@lbl.gov; Robert O. Ritchie: roritchie@lbl.gov; Tamara Alliston: tamara.alliston@ucsf.edu

[1]Department of Orthopaedic Surgery, University of California San Francisco, CA, USA

[2]School of Engineering Sciences, University of Southampton, UK

[3]Lawrence Berkeley National Laboratory, Berkeley, CA, USA

[4]Department of Materials Science and Engineering, University of California, Berkeley, CA, USA

[5]Imperial College, London, UK

[6]Department of Bioengineering and Therapeutic Sciences, Department of Otolaryngology, Eli and Edythe Broad Center for Regeneration Medicine and Stem Cell Research, University of California San Francisco, CA, USA

Abstract

The ability of bone to resist catastrophic failure is critically dependent upon the material properties of bone matrix, a composite of hydroxyapatite, collagen type I, and noncollagenous proteins. These properties include elastic modulus, hardness, and fracture toughness. Like other aspects of bone quality, matrix material properties are biologically-defined and can be disrupted in skeletal disease. While mineral and collagen have been investigated in greater detail, the contribution of noncollagenous proteins such as osteopontin to bone matrix material properties remains unclear. Several roles have been ascribed to osteopontin in bone, many of which have the potential to impact material properties. To elucidate the role of osteopontin in bone quality, we evaluated the structure, composition, and material properties of bone from osteopontin-deficient mice and wild-type littermates at several length scales. Most importantly, the results show that osteopontin deficiency causes a 30% decrease in fracture toughness, suggesting an important role for OPN in preventing crack propagation. This significant decline in fracture toughness is independent of changes in whole bone mass, structure, or matrix porosity. Using nanoindentation and quantitative backscattered electron imaging to evaluate osteopontin-deficient bone matrix at the micrometer level, we observed a significant reduction in elastic modulus and increased variability in calcium concentration. Matrix heterogeneity was also apparent at the ultrastructural level. In conclusion, we find that osteopontin is essential for the fracture toughness of bone, and reduced toughness in osteopontin-deficient bone may be related to the increased matrix heterogeneity observed at the micro-scale. By exploring the effects of osteopontin-deficiency on bone matrix material properties, composition and organization,

Corresponding Author: Tamara Alliston, Department of Orthopaedic Surgery, University of California San Francisco, 533 Parnassus, UC Hall 452, San Francisco, CA 94143-0514, Tel: 415-502-6523, Fax: 415-476-1128, tamara.alliston@ucsf.edu.

this study suggests that reduced fracture toughness is one mechanism by which loss of noncollagenous proteins contribute to bone fragility.

Keywords

Osteopontin; Rodent; Fracture Toughness; Bone-Matrix Properties; Mineralization

Introduction

Currently, bone mineral density (BMD) is the most common diagnostic used to assess fracture risk [1,2], yet less than half of non-vertebral fractures can be explained by BMD alone [3]. The limitations of using solely BMD for the prediction of fracture risk can even be shown *in vitro*. The mechanical competence of healthy human bone is compromised when exposed to chemical treatments that affect the organic matrix but not BMD [4-7]. These findings are not surprising given that the inorganic mineral is only one of several constituents that make up the complex hierarchical composite that is bone. To better reflect these complexities, the scientific and medical communities have adopted the term “bone quality” to summarize the aspects of bone that contribute to fracture risk but are not encompassed by BMD measurements [8]. Bone quality, the subject of growing interest and research efforts, comprises a number of parameters such as the microarchitecture of trabecular bone, prevalence of microcracks, bone geometry and, importantly, bone matrix material properties.

Bone matrix material properties, including elastic modulus, hardness, and fracture toughness, reflect the ability of bone to resist deformation and catastrophic failure. Even without changes in bone mass, average mineralization or bone shape, the alteration of bone matrix material properties can dramatically impact the mechanical competence of bone. For example, it is known clinically that defects in bone matrix material properties due to increased collagen cross-linking likely contributes to bone fragility in diabetes [9,10], whereas collagen point mutations contribute to bone fragility in osteogenesis imperfecta [11]. Even in healthy tissue, bone matrix material properties are biologically regulated [12,13] and anatomically distinct [14]. Bone-specific material properties are present across multiple species, suggesting that their regulation is functionally advantageous and evolutionarily conserved. However, the mechanisms that specify the material properties of bone matrix remain largely unknown.

Bone matrix is a composite of osteoblast-derived collagen and noncollagenous proteins (NCPs) that undergoes mineralization. Both the mineral and organic components of bone matrix contribute to its characteristic hardness and toughness, and defects in the composition or organization of either can cause bone fragility. While the roles of mineral and of collagen type I in bone quality have been investigated in some detail [15-20], we know little about the influence of the noncollagenous proteins on bone matrix material properties. Noncollagenous proteins such as osteocalcin, osteopontin (OPN) and others comprise a relatively small percentage of the bone matrix volume or weight, but they may contribute to bone matrix quality in a number of ways. Noncollagenous proteins control hydroxyapatite crystal nucleation, growth, shape and size as well as facilitate attachment between the major organic (collagen) and inorganic (hydroxyapatite) phases [21-26]. In addition to their effects on mineral, it has more recently been suggested that the intrinsic properties of certain NCPs could also be important for the material properties of bone matrix [27]. Networks of highly phosphorylated proteins such as OPN exhibit a molecular self-healing character allowing them to repeatedly dissipate large amounts of energy when loaded in tension [6]. Such protein networks were also found to have an energy storage mechanism and, importantly, exhibit large cohesion and toughness [28]. Hence, the role of NCPs, particularly OPN, as determinants of bone matrix material properties and fracture resistance warrants further study.

Although OPN deficiency has previously been shown to impair the macro-mechanical properties of whole bones, the mechanism for this impairment remain unclear. Duvall et al. [29] found a decreased maximum load and torque, as well as work to failure in OPN deficient mice, but these tests do not explore the underlying changes in bone matrix material properties and ultrastructure. Therefore, the origin of the effect of OPN on bone quality is unclear, which is in part due to the multiple roles attributed to it. OPN facilitates osteoclast attachment and guides mineral deposition by influencing crystal shape and size [23,25,30]. OPN, as well as other noncollagenous proteins, are enriched in cement lines, lamellar interfaces, and interfibrillar spaces of mineralized collagen fibrils [31-34]. High-resolution imagery shows that bone ultimately fails through delamination of mineralized collagen fibrils [6,35-37]. Therefore, perturbation of either the mineral or organic components at these interfaces due to genotype, such as OPN-deficiency, or disease, such as osteoporosis, could dramatically impact fracture resistance. Therefore, we hypothesized that OPN, because of its effects on bone mineral and its localization in interfibrillar spaces, is critical for the material properties of bone matrix.

In order to investigate this hypothesis, bones of male OPN-deficient (OPN -/-) mice and wild-type littermates (WT) were evaluated to determine the role of OPN in bone structure, composition, and mechanical and material behavior. Our most important result was a significant decrease in fracture toughness due to OPN deficiency. Fracture toughness is influenced by a multitude of factors including uncracked-ligament bridging, microcracking, crack deflection, and porosity [38-40]. As these factors arise at multiple length-scales, our analysis extended from the whole bone level down to the composition and organization of individual matrix constituents.

Materials and Methods

Mice

Osteopontin-deficient mice (OPN-/-) on a C57BL/6 background were purchased from the Jackson Laboratory [41]. Protocols were performed as approved by the Institutional Animal Care and Use Committee. Male mice were sacrificed at 8 weeks of age. Harvested hind limbs were cleaned of soft tissue. Left tibiae were stored in Hanks' balanced salt solution (HBSS) containing 0.05% NaN_3 at 4°C for a maximum of 5 days, whereas all other bones were wrapped in HBSS soaked gauze and stored in sealed plastic pouches at -80°C.

Fracture Toughness

Dissected femora from 9 mice of each genotype were tested in bending to measure the fracture toughness. For such measurements, ASTM standards [42] require that fracture is initiated from a sharp precrack. Generally, this is achieved by fatigue precracking, but this is not really feasible for small mouse bones. Because of this, machined notches have often been used, but more often than not, these are not sharp enough to obtain an accurate toughness measurement. Accordingly, we use a micro-notching technique here, where machined notches are sharpened by “polishing” with a razor blade using 1 μm diamond polishing solution to cut the bone midshaft through the posterior wall of the femur. The resulting micro-notches were maintained at ~ 1/3 of the bone diameter in length with a reproducible notch root radius of ~10 μm [43]. In this study, femora were tested in 37°C HBSS in a three-point bending configuration with a custom-made rig for the ELF 3200 mechanical testing machine (ELF3200, EnduraTEC, Minnetonka, MN), in general accordance with ASTM Standard E-399 [42] and E-1820 [44] and as discussed in previously developed methods for small animal bone testing [43]. Testing was conducted in displacement control at a cross-head displacement rate of 0.001 mm/s. Half-crack angle at point of instability was determined by scanning electron microscopy. Fracture toughness, K_c, was calculated using a stress-intensity solution for a circumferential through-

wall flaw in cylinders [45]. This methodology and its motivations are discussed in more detail by Ritchie et al. [43].

Areal Bone Mineral Density (aBMD) Measurement

aBMD of dissected spines (N=9 WT, 11 OPN-/-) and femurs (N=6 WT, 7 OPN-/-) was measured using a PIXImus mouse densitometer (GE Lunar II, Faxitron Corp., Wheeling, IL). Importantly, it should be noted that this areal BMD measurement is a combined measure of tissue mineral content as well as the structural organization of bone.

Micro-Computed Tomography

Dissected femora from 6 mice of each genotype were subjected to micro-computed tomography to determine cortical thickness. Femora were scanned fully hydrated in a benchtop CT 160Xi tomography system (XTEK, Tring, UK) using an acceleration voltage of 75 kV and a current of 60 mA. 1920 projections were recorded for each bone. Bone was segmented from reconstructed volumes using an adaptive threshold algorithm [46], from which the region of interest (ROI) containing only the midshaft of each bone was chosen for quantitative analysis. Segmentation and processing of ROIs was done using algorithms programmed in IDL (ITT, Boulder, CO). As each slice was roughly perpendicular to the long axis of the bone, a 2D component labeling algorithm allowed detection of the main bone compartment as well as the medullary cavity and outside void space. A thickness map of the cortical bone was obtained by filling the outside void space and performing a 3D distance transformation. The individual thickness values were obtained from the outermost voxels of the cortical bone surface using a morphological erosion, which allowed determination of average cortical bone thickness.

Synchrotron Radiation Micro-Computed Tomography

Femora from 2 mice of each genotype were tomographically imaged using synchrotron radiation. These experiments were performed at Beamline ID19 of the European Synchrotron Radiation Facility (ESRF). A 2 mm long region of the midshaft of each femur was scanned, as described in [47], at a photon energy of 20 keV and a voxel size of 1.4 μm. Histograms of reconstructed volumes were bimodal distributions with peaks representing either bone or void space. For each sample, the peak representing bone was fitted with a Lorentzian function and analyzed in terms of peak position and full width at half maximum (FWHM), which represent average calcium concentration and calcium concentration variability, respectively. In addition, the volumes were processed for bone porosity using both IDL and ImageJ. In brief, bone was segmented using an adaptive threshold algorithm [46]. Subsequently the volumes were subjected slice by slice to a 2D component labeling algorithm in order to suppress noise arising from soft tissue remnants on the outside surface of the bone as well as in the medullary cavity. Using morphological operators, all internal voids were filled. The resulting closed bone space was used as a mask on the original volumes containing only the main bone component. The resulting volume contained only the void spaces, which were analyzed using a component labeling algorithm that was programmed to return voids larger than 274 μm^3. Detected particles were ordered by size and a particle size distribution curve was computed. From these data we computed BV/TV values for the cortical bone as well as the ratios of lacuna pore space (PS_{LAC}) and blood vessel pore space (PS_{VES}) to the total pore space (PS). Based on the particle distribution curves, the size threshold for blood vessels was set at 1098 μm^3.

Nanoindentation

Dissected tibiae from 4 mice of each genotype were encased in a 2-component epoxy (Stycast 1266, Emerson & Cuming, Henkel, Dusseldorf Germany) without infiltration. Bones were sectioned with a diamond wafering blade at the midshaft perpendicular to the long axis to generate cortical bone surfaces for nanoindentation. Retrieved sections were polished with

sandpaper and diamond suspensions down to a particle size of 0.25 μm. Naonindentation was performed as described in dry conditions with a Triboindenter (Hysitron, Minneapolis, MN) equipped with a Berkovich tip [12]. Indents were applied using a trapezoidal loading profile with a loading rate of 100 μN/second, peak load of 600 μN, and a hold period of 10 seconds. From the resulting load-deformation curves, local elastic modulus was calculated as described [48]. Three sets of 10 nanoindentation points were performed in a line with a 5 μm separation. Mean values for each mouse were averaged to determine the average and standard errors for elastic modulus and hardness for each genotype.

Quantitative Back Scattering Imaging (qBEI)

Sections of tibial cortical bone adjacent to those used for nanoindentation were carbon-coated in preparation for qBEI. QBEI images for each of 5 bones for each genotype were acquired using a Hitachi S-4300SE/N environmental scanning electron microscope (ESEM) (Hitachi America, Pleasanton, CA) at 20keV electron beam energy and 1000X magnification under high-resolution image mode as described in [49]. For each bone, three images of mid-cortical bone matrix were taken in regions that generally corresponded to those tested by nanoindentation. As described in detail by Roschger et al. [49], grayscale values from QBEI images were calibrated using hydroxyapatite and carbon standards (MAC Consultants, St. Ives, UK) and beam current was controlled using a Faraday cup in then center of the standard. Fitting the bone mineral density distribution with a Gaussian curve allowed determination of the calcium concentration (weight %) and variability. Graphs indicate the mean and standard error of values for 5 mice, each of which reflects the mean of the three qBEI measurements.

Small Angle X-ray Scattering (SAXS)

Tibiae from 4 wild-type and 3 OPN-/- mice were thawed, air-dried and embedded in a 2-component epoxy (Stycast 1266). Embedded tibiae were sectioned parallel to their long axis using a diamond wafering blade. Cut sections were thinned to approximately 300 μm in thickness using a polishing wheel. SAXS patterns for several sections of the cortical bone were acquired using a benchtop system with Cu Kα radiation (Nanostar, Bruker, Madison, WI) as well as a dedicated experiment at beamline 8.3.3 at the Advanced Light Source (ALS) at the Lawrence Berkeley National Laboratory using an X-ray energy of 10 KeV. Acquired patterns were absorption-corrected and azimuthally integrated to calculate mean crystal thickness [50]. Values using these two approaches were pooled.

Transmission Electron Microscopy (TEM)

Two methods of sectioning were chosen: Ultramicrotomy (UM) and Focused Ion Beam Milling (FIB). 1. Ultramicrotomy: Additional tibiae from 2 mice of each genotype were fixed in anhydrous ethylene glycol for 24 hr, dehydrated by rinsing in 100% ethanol three times for 5 min in acetonitrile, and then infiltrated with resin (Agar Scientific) over several days. Mounting resin was prepared with 12 g Quetol, 6.5 g methyl nadic anhydride (MNA), 15.5 g nonenylsuccinic anhydride (NSA), and 0.7 g benzlydimethylamine (BDMA). The samples were agitated at room temperature in 1:1 solutions of acetonitrile and resin for 1 day, then 1:2 acetonitrile resin for 1 day, and finally 100% resin for 3 days under vacuum; the resin was changed every 24 hr. Samples were then cured in fresh resin for 24 hr at 60°C. Silver to gold sections (70–90 nm) were cut onto distilled water with an ultramicrotome using a 35 degree diamond knife. Samples were collected immediately on lacy carbon 300 mesh copper grids. 2. Focussed ion beam milling: For each of 2 tibiae per genotype, focused ion beam milled sections of approximately 80 nm thickness were prepared using FIB 200 (FEI Company, Hillsboro, OR) which is a single focused gallium ion beam (FIB) instrument. The samples were first coated with approximately 40-50 nm of gold to minimize specimen charging during FIB-milling. Before milling, a platinum layer, 20 μm × 2.5 μm and 1 μm thick, was deposited over

the area of interest on each of the two coated samples. Thin sections were prepared parallel to the long axis of the samples. The FIB ion beam was operated at 30 kV with beam currents that ranged from 3 nA to 100 pA with the lower current used for final polishing of the electron-transparent portion of the sample.

For TEM analysis, bright field imaging was performed on a JEOL 2000 FX TEM using operating voltages of 120 and 200 kV. Multiple longitudinal and transverse sections were investigated for each bone to assess nanoscale tissue organization. Quantitative analyses included measurement of hydroxyapatite dimensions, collagen fibril diameter and D-banding. To study the collagen fibril diameter, selected sections where decalcified in 5% ethylene-diaminetetra-acetic acid (EDTA) disodium salt (Sigma, St. Louis, MO) in 0.1 M Pipes buffer (pH 7.4) for 15 minutes. The decalcified sections were subsequently stained with uranyl-acetate and lead citrate for 5 minutes in each. The collagen fibril banding pattern was also evident in non-stained TEM sections prepared by FIB.

The thickness of the crystals was measured from TEM images using methods described in [51]. Crystals were observed both on edge and *en face* within the mineralized collagen fibrils. Crystals oriented *en face* were plate-like in shape with no well defined profile, whereas crystals on edge were needle-shaped with a well defined, oblong profile. The plate-like dimension of the crystals could not be determined accurately due the scarcity of clearly visible plate-like crystals. In comparison, the needle-like crystals were generally uniform and much easier to isolate and measure. The thickness of these needle-like crystals were measured for both UM and FIB prepared OPN-/- and WT bone sections using N=50 for apatite thickness.

In order to confirm the 3D morphology of the crystals and the supposition that differences in contrast observed from the crystals observed on edge and *en face* arises from differences in their orientation, tilting experiments were performed. Nine images were taken with a variation of tilt angles ranging from -20° to +20° with 5° increments. Ultramicrotomy prepared WT and OPN-/-were imaged to determine a difference in 3D morphology of crystal apatite. These tilting experiments confirmed that the needle-like crystals were actually plate-like crystallites viewed on edge.

Demineralized Bone Testing

Dissected femora from 5 mice of each genotype were thawed and cut at both ends to permit flushing with HBSS to remove bone marrow. The samples were demineralized in a 19% EDTA solution containing 0.05% NaN_3, 2 μg/ml leupeptin and 2 μg/ml aprotinin for 3 days. Subsequently, the samples were soaked in 110 mM NaCl, 40 mM $CaCl_2$, and 10 mM HEPES overnight, after which they were prepared for tensile testing according to Silva et al. [19]. Tensile testing was performed in 20°C HBSS using custom grips and a small scale mechanical tester (ELF3200, Bose) at a displacement rate of 0.1 mm/s. Digital video recordings of the specimens, marked with Verhoeff's stain at two points, allowed determination of strain in the gauge region of the samples using a custom algorithm (Labview 8.6, National Instruments, Austin, TX), from which tensile strength and elastic modulus were calculated. Sample width was determined from digital images. Thickness was based on measurements using a pair of calipers and micro-CT. In brief, we compared cortical thickness of a set of mineralized femora determined using micro-CT and image processing, including a distance transform, with cortical thickness of a set of demineralized femora determined using a pair of calipers and found good agreement of average thicknesses without any significant differences between the two methods. Therefore, calipers were used measure cortical thickness of the remaining demineralized samples used for tension testing in order to minimize protein degradation due to ambient exposure.

Statistics

Statistical comparisons of data for OPN-/- and WT mouse bones were compared using two tailed Student's T-test using a significance threshold of p=0.05.

Results

Reduced fracture toughness in OPN-deficient bone

Bone's fracture resistance is significantly derived from its ability to impede the propagation of cracks once a fracture is initiated [52]. Fracture toughness testing measures a material property of bone, specifically the ability of a bone to resist crack propagation independently of its ability to resist crack initiation. To determine if OPN is important for the ability of bone to resist crack propagation, dissected femora from wild-type and OPN-/- mice were prepared for fracture toughness testing. Femora were notched at the mid-diaphysis and loaded to failure in a three-point bending configuration (Figure 1A). The fracture toughness of wild-type femora (K_c = 5.55 ± 1.78 MPa $m^{1/2}$) was consistent with previously reported values [12,43]. However, the fracture toughness of OPN-/- femora (3.87 ± 0.79 MPa $m^{1/2}$) was 30% lower than wild-type values ($p<0.05$, Figure 1B). This result is significantly above the coefficient of variation (18%) for analysis of fracture toughness in mouse bone. Therefore, the reduced fracture toughness indicates that OPN deficiency compromises the ability of bone to resist crack propagation.

Though the reduced fracture toughness of the OPN-deficient bone likely contributes to the bone fragility reported by Duvall et al. [29], the mechanisms by which OPN contributes to fracture toughness remain unclear, in part due to the multiplicity of roles for this protein. For example, OPN has been previously been shown to influence bone remodeling [53] and mineral crystallization [54], both of which may impact the ability of bone to resist fracture. In an effort to better understand the contribution of the OPN protein to the mechanical competence of bone, the structural and material properties of bone from OPN-deficient mice were investigated at multiple length scales.

Loss of fracture toughness is not accompanied by loss of bone mass or cortical thickness

At the largest length scale, bone mass and structure influence the ability of bone to resist fracture. Accordingly, DEXA and micro-CT analysis were used to evaluate bone mass and structure in wild-type and OPN-deficient mice. DEXA analysis showed a significant increase in the aBMD of the OPN-deficient mouse spine, which is composed primarily of trabecular bone (Figure 2A). Since OPN-deficient mice have previously been reported to possess increased trabecular bone volume [55], this observation validated the OPN-deficient phenotype of the mice used in this study. However, OPN-dependent differences in areal aBMD were not apparent in femora (Figure 2B). The structural features of cortical bone were examined more carefully using micro-CT since this is the region that was assayed in fracture toughness tests. The cortical thickness of OPN-deficient femora (318 ± 36 μm) did not differ significantly from that of wild-type bones (303 ± 28 μm), (Figures 2C, 2D), a finding that is consistent with Koyama, et al. [56]. Hence, there are no macroscopic changes in cortical bone mass or geometry which could be responsible for the OPN-dependent reduction in fracture toughness.

Absence of changes in porosity in OPN-deficient mice

Microstructural features such as microcracks or changes in bone porosity can impact the fracture toughness of bone. To assess the effect of OPN-deficiency on cortical bone porosity, bones were examined by synchrotron radiation micro-computed tomography (SRμCT). Figures 3A and 3B show reconstructed slices of cortical bone from wild-type and OPN-deficient femora, respectively. Quantitative analyses revealed no significant differences in overall cortical bone volume or porosity (BV/TV_{WT} 0.9386 ± 0.0011, $BV/TV_{OPN-/-}$ 0.9317 ±

0.0042), (Figure 3C). Reconstructed images, such as the example shown in Figure 3D, were used to evaluate the distribution of pore size. A threshold set based on pore size was used to distinguish between osteocyte lacunae which represent approximately 47-48% of the pore volume (Figure 3F), and blood vessels which comprise the remaining 52-53% (Figure 3G). No differences in the distribution of pores for osteocyte lacunae or vasculature were observed between wild-type and OPN-deficient mice (Figure 3H). In addition, pore organization also appeared to be very similar with no evidence of the qualitatively striking differences in blood vessel or lacunae organization that were reported by Schneider et al. [47]. Therefore, the loss of fracture toughness in OPN-deficient bones is also not a result of microstructural defects in porosity.

OPN-deficiency results in decreased indentation modulus

This suggests that the factors responsible for the reduced fracture toughness were independent of bone size and shape. Several proposed mechanisms for bone toughening occur at smaller length scales. Therefore, we analyzed bones from WT and OPN-deficient mice using several higher resolution approaches. Nanoindentation was used to evaluate the local material properties of tibial cortical bone matrix. The hardness reflects the ability to resist plastic deformation whereas the indentation modulus reflects the ability of the mineral/protein composite to resist elastic deformation. Although bone matrix hardness did not differ between wild-type and OPN-deficient mice, the indentation modulus for OPN-deficient mice was reduced to 20.3 ± 1.0 GPa compared to 23.9 ± 1.7 GPa ($p<0.05$, Figure 4A). The 15% decrease in indentation modulus in OPN-deficient mice is consistent with the recent observations of Kavukcuoglu, et al [57].

Increased calcium variability in osteopontin-deficient bone matrix

Defects in either the mineral or the organic matrix can alter the indentation modulus. To relate the changes in local indentation modulus to changes in local mineral content, cross-sections of wild-type and OPN-deficient tibial cortical bone were evaluated by quantitative backscattered electron imaging (qBEI). This approach was chosen because it queries bone matrix at the same length scale as nanoindentation; nanoindentation probes matrix material properties in the superficial 4 μm, whereas QBEI, at 20 keV electron energy, quantifies the mineral concentration of the superficial 2 μm of the section [58]. Figures 5A and 5B show representative qBEI images from wild-type and OPN-deficient bone matrix, each of which approximately corresponds to the sites of nanoindentation. Interestingly, significant differences in average matrix calcium concentration were not apparent (Figure 5C). However, the average full width at half maximum (FWHM) of the bone mineral density distribution curves was increased by 5% to 2.89 ± 0.06 wt%Ca in OPN-deficient bone compared to 2.76 ± 0.05 wt%Ca in the WT bone, demonstrating an increase in calcium variability (Figure 5D). Therefore, OPN-deficient bone matrix has a significantly higher variability of calcium concentration. Though not significantly different, a similar trend was observed by SRμCT (Figure 5E).

A combination of in vitro and in vivo studies has implicated OPN in the control of mineral crystal maturity and size [23,53,54,59]. Therefore, we hypothesized that OPN-deficiency might have more significant effects on crystal organization and size than it did on mineral concentration. Small angle X-ray scattering (SAXS) was performed to evaluate the effect of OPN-deficiency on bone matrix mineral organization. In SAXS, changes in the symmetry of the diffraction pattern indicate altered organization of the matrix, whereas the t-parameter can be used to determine crystal thickness. Osteopontin-dependent differences were not apparent either in the distinct diffraction features originating from the collagen D-banding or in the ellipsoid pattern originating from the alignment of the mineral crystals along the long axis of

the bone (Figure 6A). Figure 6B shows the quantitative analysis of mean crystal thickness in OPN-deficient bone matrix relative to WT matrix.

To examine the effect of OPN deficiency on bone matrix organization, transmission electron microscopy studies were performed. However, these studies did not provide conclusive evidence with regards to differences in collagen organization (Figure 6) in OPN-deficient bone or changes in apatite length, collagen fibril width, or collagen fibril banding (Table 1). So whilst bone matrix did show increased heterogeneity in qBEI images (Figure 5) a similar increase in heterogeneity could not be detected at the ultrastructural level.

Tension testing of demineralized osteopontin-deficient bone matrix

The subtle differences in matrix mineralization in OPN-deficient mice suggested that the OPN protein itself might contribute to the mechanical properties of bone. *In vitro* studies have shown that OPN can form self-healing networks with very high toughness that might be important for the material properties of bone, independently of the role of OPN in regulating mineral deposition [28,60]. To examine the role of OPN in bone matrix material properties in the absence of mineral, test specimens were cut in a standard geometry from demineralized femora of wild-type and OPN-deficient mice [19]. Specimens evaluated in tension tests showed no differences in ultimate peak tensile strength or elastic modulus (Figure 7). Although an intrinsic contribution of the OPN protein to the mechanical behavior of bone matrix was not detectable at the macro-scale, studies on smaller scale specimens or in different geometries may be more informative.

Discussion

By combining approaches that assess the material properties and composition at different levels of bone hierarchy, the present results reveal that OPN participates in establishing bone matrix material properties. Most notably, OPN deficiency results in 30% decreased fracture toughness, suggesting an important role for OPN in impeding crack propagation. This marked decline in fracture toughness was independent of changes in whole bone mass, structure, or matrix porosity. The search for mechanisms potentially responsible for the loss of fracture toughness revealed that OPN-deficient cortical bone has a significantly reduced indentation modulus. Though the reduction in modulus did not correspond to local changes in mineral concentration, the mineralization and ultrastructural organization of OPN-deficient bone matrix was more heterogeneous. Some of these features resemble the compositional and mechanical properties of osteoporotic bone matrix, which also exhibits a significant loss of toughness [18]. In conclusion, we find that OPN is essential for the fracture toughness of bone. By exploring the effects of OPN-deficiency on bone matrix material properties, composition and organization, this study narrows the search for mechanisms by which OPN toughens bone, and how toughness is lost in skeletal disease such as osteoporosis.

The results of this study extend and confirm previous observations that OPN plays a critical role in the mechanical behavior of bone. The reduced fracture toughness in the current study likely contributes to the decreased work to failure observed by Duvall, et al [29]. Work to failure indicates the ability of bone to resist both crack initiation and crack propagation, whereas our fracture toughness measurements evaluate resistance to crack propagation. Since microcracks invariably pre-exist in bone, the latter measurements represent a more appropriate measure of resistance to fracture. Therefore, at least part of the impaired work to failure is due to the role of OPN in impeding crack propagation. Similar to Kavukcuoglu et al. [57], our nanoindentation studies showed a decrease in elastic modulus. Although Duvall et al., reported an increase in elastic modulus in OPN-deficient bone matrix, this value was ascertained in whole bone three-point bending studies. Differences between elastic modulus values measured by nanoindentation and those acquired by three-point bending have previously been reported

[61]. Such differences can be explained by the anisotropic properties of bone and the contribution of hierarchical structural elements that influence mechanical behavior when going from the nanoor micrometer level to the whole bone. While elastic modulus and fracture toughness are related, the dependence of elastic modulus on fracture toughness is not linear, which suggests that the smaller decrease in elastic modulus in OPN-deficient bone alone cannot explain the detected decrease in fracture toughness.

The reduced fracture toughness of OPN-deficient bone is also not explained by structural changes. Fracture toughness tests evaluate the material properties of cortical bone, which showed no difference in cortical thickness or bone volume. The fact that we did not detect such changes in cortical bone suggests that growth and development in OPN-deficient mice is normal, which is in accordance with previous communications [62]. In contrast, spine aBMD, representing primarily of trabecular bone, was increased. aBMD is a combined measure of both structure tissue mineral content and represents, in the case of the spine, primarily trabecular bone, due to its high volume fraction in vertebrae. Trabecular bone is most sensitive to changes in osteoclast activity, which is significantly affected by OPN deficiency [55]. Another important structural parameter to consider in cortical bone is the porosity and pore size distribution. Pores detected by SRμCT may result from lacunae, vasculature or microdamage [47,63]. Marked changes in pore size distribution or organization could critically influence the ability of cortical bone to resist crack propagation. As our data show, however, no such changes are present in OPN-deficient femora suggesting that the effect of OPN on fracture toughness is not due to changes in the size distribution or organization of pores in cortical bone.

Progressing to the micrometer length scale, qBEI and nanoindentation provide information on local mineral content and material properties. Although local elastic modulus typically correlates with the local mineral concentration, the decreased elastic modulus in OPN-deficient bone matrix was not accompanied by a reduction in calcium concentration. Instead, QBEI detected a significant increase in calcium variability in OPN-deficient bone matrix. Interestingly, this increased heterogeneity of OPN-deficient bone corresponds to recent observations by Busse et al [18]. These authors investigated the properties of single trabeculae from bone biopsies of healthy and osteoporotic patients. They reported an increase in mean calcium concentration and heterogeneity in osteoporotic trabeculae, which was accompanied by a decrease in elastic modulus and energy to failure, as determined from three-point bending tests. Furthermore, Grynpas et al. observed a marked decrease in certain NCP fractions in osteoporotic bone [64]. The extent to which changes in osteoclast activity in OPN-deficient mice, or in osteoporosis, are responsible for the altered bone matrix material properties remains unclear and is an important area for future research. Collectively, current studies suggest that loss of noncollagenous proteins such as OPN may contribute to osteoporosis by compromising bone matrix material properties.

Although fracture toughness can be affected by matrix material properties, bone structure, porosity, matrix mineralization or organization [12,52,65], this study shows that these leading potential mechanisms are insufficient to explain the reduced fracture toughness in OPN-deficient mice. An attractive area for future research will be investigating the role of cross-linking of collagenous and noncollagenous extracellular matrix proteins in the reduced fracture toughness of OPN-deficient mouse bone. Studies on diabetic, osteoporotic and aging bone highlight the potential role of collagen cross-linking in fracture toughness [9]. Transglutaminase 2 cross-links several noncollagenous proteins in bone, including osteopontin [66,67]. However, the extent to which defects in matrix protein cross-linking contribute to the reduced fracture toughness of OPN-deficient mouse bone, or in the altered size-independent mechanical properties of bones from mice exposed to physical exercise or high-fat diet [68-70], remains to be fully elucidated.

We hypothesized that the ability of OPN to form self-healing protein networks [28,60] may contribute to fracture toughness. OPN and other noncollagenous proteins, are abundant at interfibrillar interfaces and lamellar/cement lines [31-34]. Microscopic and mechanical investigations have shown that bone generally fails at these well-defined interfaces, either on the single mineralized collagen fibril level or at the lamellar/cement line [35-37,39,52,71]. Therefore it can be argued that variability, such as compositional variations, at these interfaces may influence fracture behavior and hence fracture toughness. The possibility that OPN-deficiency causes interfacial weakening and a lowered fracture toughness merits further investigation. Such a mechanistic analysis of fracture behavior could be achieved using a combination of imaging and fracture toughness testing, as in two recent studies [52,63]. In this light, it might have also been beneficial to perform tension tests perpendicular to the long axis of the bone. Due to technical limitations of sample preparation, however, this was not possible. Consequently, this study does not exclude a direct role for OPN in influencing the fracture toughness. More advanced sample preparation methods, such as laser microdissection of bone specimens [72], may enable analysis of specific bone interfaces. In addition, more advanced multiscale indentation testing, previously reported on cartilage [73], might enable the investigation of fibrillar and interfibrillar mechanical properties in demineralized bone samples.

The expression of OPN and other noncollagenous proteins, such as osteocalcin, is highly regulated throughout osteoblast differentiation. Both factors that regulate bone matrix material properties, TGF-β and glucocorticoids, also regulate OPN expression in vitro [74]. We hypothesized that OPN maybe a downstream target of TGF-β in the control of bone matrix material properties. However, the expression of OPN was not significantly altered in neonatal, 2-month old, or 6-month old transgenic mice (data not shown) that express a dominant negative TGF-β type II receptor and have increased bone matrix material properties. The downstream targets of the TGF-β and glucocrticoid pathways that are responsible for the changes in bone matrix material properties remain unknown. Since these properties are biologically regulated, anatomically distinct, and important aspects of bone quality, identifying the mechanisms by which they are established is a critical area for future investigation.

In conclusion, we find that OPN-deficiency significantly impairs the ability of bone to resist the propagation of incipient cracks, accompanied by a decrease in matrix elastic modulus and increased calcium variability. Whether the interfacial strength of micro- and nanostructural features such as cement lines, interlamellar boundaries or mineralized collagen fibrils is also impaired can neither be proven nor falsified at this stage and requires further study. Importantly, our results suggest that osteoporotic and OPN-deficient bone share some common hallmarks; in both cases, local mineral distribution is altered and leads to increased heterogeneity. Hence, the possibility of using noncollagenous proteins such as OPN as biomarkers for the mechanical competence of bone should be further investigated.

Acknowledgments

This research was supported by NIDCR R01 DE019284 and NIDCR RO3 DE16868 to TA. Funding for instrumentation was in part provided by NIH grant R01 GM65354. Funding for LS, SI-M, JWA and ROR was provided by the Office of Science, Office of Basic Energy Sciences, Division of Materials Sciences and Engineering, of the U.S. Department of Energy under Contract No. DE-AC02-05CH11231. The Advanced Light Source is supported by the Director, Office of Science, Office of Basic Energy Sciences, of the U.S. Department of Energy under Contract No. DE-AC02-05CH11231. In addition, the authors gratefully acknowledge the expertise and assistance of Prof. Ian Sinclair for synchrotron radiation micro-computed tomography, Dr. Eduardo Saiz for scanning electron microscopy as well as Dr. Alexander Hexemer and Dr. Alexander Mastroianni during the acquisition of the small angle x-ray scattering data.

References

1. Fogelman I, Blake GM. Different approaches to bone densitometry. J Nucl Med 2000;41:2015–2025. [PubMed: 11138687]
2. Lochmuller EM, Lill CA, Kuhn V, Schneider E, Eckstein F. Radius bone strength in bending, compression, and falling and its correlation with clinical densitometry at multiple sites. J Bone Miner Res 2002;17:1629–38. [PubMed: 12211433]
3. Schuit SC, van der Klift M, Weel AE, de Laet CE, Burger H, Seeman E, Hofman A, Uitterlinden AG, van Leeuwen JP, Pols HA. Fracture incidence and association with bone mineral density in elderly men and women: the Rotterdam Study. Bone 2004;34:195–202. [PubMed: 14751578]
4. Walsh WR, Guzelsu N. Compressive Properties of Cortical Bone - Mineral Organic Interfacial Bonding. Biomater 1994;15:137–145.
5. DePaula CA, Abjornson C, Pan Y, Kotha SP, Koike K, Guzelsu N. Changing the structurally effective mineral content of bone with in vitro fluoride treatment. J Biomech 2002;35:355–61. [PubMed: 11858811]
6. Kindt JH, Thurner PJ, Lauer ME, Bosma BL, Schitter G, Fantner GE, Izumi M, Weaver JC, Morse DE, Hansma PK. In situ observation of fluoride-ion-induced hydroxyapatite-collegen detachment on bone fracture surfaces by atomic force microscopy. Nanotech 2007;18:135102. 8pp.
7. Thurner PJ, Erickson B, Turner P, Jungmann R, Lelujian J, Proctor A, Weaver JC, Schitter G, Morse DE, Hansma PK. The Effect of NaF In Vitro on the Mechanical and Material Properties of Trabecular and and Cortical bone. Adv Mater 2009;21:451–457.
8. Hernandez CJ, Keaveny TM. A biomechanical perspective on bone quality. Bone 2006;39:1173–81. [PubMed: 16876493]
9. Saito M, Marumo K. Collagen cross-links as a determinant of bone quality: a possible explanation for bone fragility in aging, osteoporosis, and diabetes mellitus. Osteoporos Int. 2009
10. Vashishth D. The role of the collagen matrix in skeletal fragility. Curr Osteoporos Rep 2007;5:62–6. [PubMed: 17521507]
11. Kozloff KM, Carden A, Bergwitz C, Forlino A, Uveges TE, Morris MD, Marini JC, Goldstein SA. Brittle IV mouse model for osteogenesis imperfecta IV demonstrates postpubertal adaptations to improve whole bone strength. J Bone Miner Res 2004;19:614–22. [PubMed: 15005849]
12. Balooch G, Balooch M, Nalla RK, Schilling S, Filvaroff EH, Marshall GW, Marshall SJ, Ritchie RO, Derynck R, Alliston T. TGF-beta regulates the mechanical properties and composition of bone matrix. Proc Natl Acad Sci U S A 2005;102:18813–8. [PubMed: 16354837]
13. Lane NE, Yao W, Balooch M, Nalla RK, Balooch G, Habelitz S, Kinney JH, Bonewald LF. Glucocorticoid-treated mice have localized changes in trabecular bone material properties and osteocyte lacunar size that are not observed in placebo-treated or estrogen-deficient mice. J Bone Miner Res 2006;21:466–76. [PubMed: 16491295]
14. Currey JD. The design of mineralised hard tissues for their mechanical functions. J Exp Biol 1999;202:3285–94. [PubMed: 10562511]
15. Zioupos P, Currey JD, Hamer AJ. The role of collagen in the declining mechanical properties of aging human cortical bone. J Biomed Mater Res 1999;45:108–16. [PubMed: 10397964]
16. Fratzl P, Gupta HS, Paschalis EP, Roschger P. Structure and mechanical quality of the collagen-mineral nano-composite in bone. J Mater Chem 2004;14:2115–2123.
17. Roschger P, Paschalis EP, Fratzl P, Klaushofer K. Bone mineralization density distribution in health and disease. Bone 2008;42:456–66. [PubMed: 18096457]
18. Busse B, Hahn M, Soltau M, Zustin J, Puschel K, Duda GN, Amling M. Increased calcium content and inhomogeneity of mineralization render bone toughness in osteoporosis: mineralization, morphology and biomechanics of human single trabeculae. Bone 2009;45:1034–43. [PubMed: 19679206]
19. Silva MJ, Brodt MD, Wopenka B, Thomopoulos S, Williams D, Wassen MH, Ko M, Kusano N, Bank RA. Decreased collagen organization and content are associated with reduced strength of demineralized and intact bone in the SAMP6 mouse. J Bone Miner Res 2006;21:78–88. [PubMed: 16355276]

20. Tang SY, Zeenath U, Vashishth D. Effects of non-enzymatic glycation on cancellous bone fragility. Bone 2007;40:1144–51. [PubMed: 17257914]
21. Chen Y, Bal BS, Gorski JP. Calcium and collagen binding properties of osteopontin, bone sialoprotein, and bone acidic glycoprotein-75 from bone. J Biol Chem 1992;267:24871–8. [PubMed: 1447223]
22. Hunter GK, Goldberg HA. Nucleation of hydroxyapatite by bone sialoprotein. Proc Natl Acad Sci U S A 1993;90:8562–5. [PubMed: 8397409]
23. Hunter GK, Hauschka PV, Poole AR, Rosenberg LC, Goldberg HA. Nucleation and inhibition of hydroxyapatite formation by mineralized tissue proteins. Biochem J 1996;317(Pt 1):59–64. [PubMed: 8694787]
24. Stayton PS, Drobny GP, Shaw WJ, Long JR, Gilbert M. Molecular recognition at the protein-hydroxyapatite interface. Crit Rev Oral Biol Med 2003;14:370–6. [PubMed: 14530305]
25. Qiu SR, Wierzbicki A, Orme CA, Cody AM, Hoyer JR, Nancollas GH, Zepeda S, De Yoreo JJ. Molecular modulation of calcium oxalate crystallization by osteopontin and citrate. Proc Natl Acad Sci U S A 2004;101:1811–5. [PubMed: 14766970]
26. Tye CE, Hunter GK, Goldberg HA. Identification of the type I collagen-binding domain of bone sialoprotein and characterization of the mechanism of interaction. J Biol Chem 2005;280:13487–92. [PubMed: 15703183]
27. Fantner GE, Hassenkam T, Kindt JH, Weaver JC, Birkedal H, Pechenik L, Cutroni JA, Cidade GAG, Stucky GD, Morse DE, Hansma PK. Sacrificial bonds and hidden length dissipate energy as mineralized fibrils separate during bone fracture. Nat Mater 2005;4:612–616. [PubMed: 16025123]
28. Zappone B, Thurner PJ, Adams J, Fantner GE, Hansma PK. Effect of Ca2+ ions on the adhesion and mechanical properties of adsorbed layers of human osteopontin. Biophys J 2008;95:2939–50. [PubMed: 18586839]
29. Duvall CL, Taylor WR, Weiss D, Wojtowicz AM, Guldberg RE. Impaired angiogenesis, early callus formation, and late stage remodeling in fracture healing of osteopontin-deficient mice. J Bone Miner Res 2007;22:286–97. [PubMed: 17087627]
30. Giachelli CM, Steitz S. Osteopontin: a versatile regulator of inflammation and biomineralization. Matrix Biol 2000;19:615–22. [PubMed: 11102750]
31. McKee MD, Nanci A. Osteopontin at mineralized tissue interfaces in bone, teeth, and osseointegrated implants: ultrastructural distribution and implications for mineralized tissue formation, turnover, and repair. Microsc Res Tech 1996;33:141–64. [PubMed: 8845514]
32. Nanci A. Content and distribution of noncollagenous matrix proteins in bone and cementum: relationship to speed of formation and collagen packing density. J Struct Biol 1999;126:256–69. [PubMed: 10441531]
33. Derkx P, Nigg AL, Bosman FT, Birkenhager-Frenkel DH, Houtsmuller AB, Pols HA, van Leeuwen JP. Immunolocalization and quantification of noncollagenous bone matrix proteins in methylmethacrylate-embedded adult human bone in combination with histomorphometry. Bone 1998;22:367–73. [PubMed: 9556137]
34. Thurner PJ, Lam S, Weaver JC, Morse DE, Hansma PK. Localization of Phosphorylated Serine, Osteopontin, and Bone Sialoprotein on Mineralized Collagen Fibrils in Bone. J Adhes 2009:85.
35. Braidotti P, Bemporad E, D'Alessio T, Sciuto SA, Stagni L. Tensile experiments and SEM fractography on bovine subchondral bone. J Biomech 2000;33:1153–7. [PubMed: 10854890]
36. Braidotti P, Branca FP, Stagni L. Scanning electron microscopy of human cortical bone failure surfaces. J Biomech 1997;30:155–62. [PubMed: 9001936]
37. Thurner PJ, Erickson B, Jungmann R, Schriock Z, Weaver JC, Fantner GE, Schitter G, Morse DE, Hansma PK. High-Speed Photography of Compressed Human Trabecular Bone Correlates Whitening to Microscopic Damage. Engineer Fracture Mech 2007;74:1928–1941.
38. Vashishth D, Behiri JC, Bonfield W. Crack growth resistance in cortical bone: concept of microcrack toughening. J Biomech 1997;30:763–9. [PubMed: 9239560]
39. Nalla RK, Kinney JH, Ritchie RO. Mechanistic fracture criteria for the failure of human cortical bone. Nat Mater 2003;2:164–8. [PubMed: 12612673]
40. Yeni YN, Brown CU, Wang Z, Norman TL. The influence of bone morphology on fracture toughness of the human femur and tibia. Bone 1997;21:453–9. [PubMed: 9356740]

41. Liaw L, Birk DE, Ballas CB, Whitsitt JS, Davidson JM, Hogan BL. Altered wound healing in mice lacking a functional osteopontin gene. J Clin Invest 1998;101:1468–78. [PubMed: 9525990]
42. E399 Standard test method for plane-strain fracture toughness of metallic materials. Philadelphia, PA: Am Soc Test Mater; 1990.
43. Ritchie RO, Koester KJ, Ionova S, Yao W, Lane NE, Ager JW 3rd. Measurement of the toughness of bone: a tutorial with special reference to small animal studies. Bone 2008;43:798–812. [PubMed: 18647665]
44. E1820 Standard test method for measurement of fracture toughness. West Conshohocken, PA: Am Soc Test Mater; 2006.
45. Zahoor, A. Ductile Fracture Handbook. Palo Alto: E.P.R. Institute; 1989. Circumferential Throughwall Cracks.
46. Ridler TW. Picture thresholding using an iterative selection method. IEEE Trans Syst Man Cybern 1978;8:630–632.
47. Schneider P, Stauber M, Voide R, Stampanoni M, Donahue LR, Muller R. Ultrastructural properties in cortical bone vary greatly in two inbred strains of mice as assessed by synchrotron light based micro- and nano-CT. J Bone Miner Res 2007;22:1557–70. [PubMed: 17605631]
48. Oliver WC, Pharr GM. An Improved Technique for Determining Hardness and Elastic-Modulus Using Load and Displacement Sensing Indentation Experiments. J Mater Res 1992;7:1564–1583.
49. Roschger P, Fratzl P, Eschberger J, Klaushofer K. Validation of quantitative backscattered electron imaging for the measurement of mineral density distribution in human bone biopsies. Bone 1998;23:319–26. [PubMed: 9763143]
50. Fratzl P, Schreiber S, Roschger P, Lafage MH, Rodan G, Klaushofer K. Effects of sodium fluoride and alendronate on the bone mineral in minipigs: a small-angle X-ray scattering and backscattered electron imaging study. J Bone Miner Res 1996;11:248–53. [PubMed: 8822349]
51. Rubin MA, Jasiuk I, Taylor J, Rubin J, Ganey T, Apkarian RP. TEM analysis of the nanostructure of normal and osteoporotic human trabecular bone. Bone 2003;33:270–82. [PubMed: 13678767]
52. Koester KJ, Ager JW 3rd, Ritchie RO. The true toughness of human cortical bone measured with realistically short cracks. Nat Mater 2008;7:672–7. [PubMed: 18587403]
53. Shapses SA, Cifuentes M, Spevak L, Chowdhury H, Brittingham J, Boskey AL, Denhardt DT. Osteopontin facilitates bone resorption, decreasing bone mineral crystallinity and content during calcium deficiency. Calcif Tissue Int 2003;73:86–92. [PubMed: 14506959]
54. Boskey AL, Spevak L, Paschalis E, Doty SB, McKee MD. Osteopontin deficiency increases mineral content and mineral crystallinity in mouse bone. Calcif Tissue Int 2002;71:145–54. [PubMed: 12073157]
55. Yoshitake H, Rittling SR, Denhardt DT, Noda M. Osteopontin-deficient mice are resistant to ovariectomy-induced bone resorption. Proc Natl Acad Sci U S A 1999;96:8156–60. [PubMed: 10393964]
56. Koyama Y, Rittling SR, Tsuji K, Hino K, Salincarnboriboon R, Yano T, Taketani Y, Nifuji A, Denhardt DT, Noda M. Osteopontin deficiency suppresses high phosphate load-induced bone loss via specific modulation of osteoclasts. Endocrinol 2006;147:3040–9.
57. Kavukcuoglu NB, Denhardt DT, Guzelsu N, Mann AB. Osteopontin deficiency and aging on nanomechanics of mouse bone. J Biomed Mater Res A 2007;83:136–44. [PubMed: 17390367]
58. Howell PG, Boyde A. Monte Carlo simulations of electron scattering in bone. Bone 1994;15:285–91. [PubMed: 8068449]
59. Boskey AL, Maresca M, Ullrich W, Doty SB, Butler WT, Prince CW. Osteopontin-hydroxyapatite interactions in vitro: inhibition of hydroxyapatite formation and growth in a gelatin-gel. Bone Miner 1993;22:147–59. [PubMed: 8251766]
60. Fantner GE, Adams J, Turner P, Thurner PJ, Fisher LW, Hansma PK. Nanoscale ion mediated networks in bone: osteopontin can repeatedly dissipate large amounts of energy. Nano Lett 2007;7:2491–8. [PubMed: 17645366]
61. Silva MJ, Brodt MD, Fan Z, Rho JY. Nanoindentation and whole-bone bending estimates of material properties in bones from the senescence accelerated mouse SAMP6. J Biomech 2004;37:1639–46. [PubMed: 15388305]

62. Rittling SR, Matsumoto HN, McKee MD, Nanci A, An XR, Novick KE, Kowalski AJ, Noda M, Denhardt DT. Mice lacking osteopontin show normal development and bone structure but display altered osteoclast formation in vitro. J Bone Miner Res 1998;13:1101–11. [PubMed: 9661074]
63. Voide R, Schneider P, Stauber M, Wyss P, Stampanoni M, Sennhauser U, van Lenthe GH, Muller R. Time-lapsed assessment of microcrack initiation and propagation in murine cortical bone at submicrometer resolution. Bone 2009;45:164–73. [PubMed: 19410668]
64. Grynpas MD, Tupy JH, Sodek J. The Distribution of Soluble, Mineral-Bound, and Matrix-Bound Proteins in Osteoporotic and Normal Bones. Bone 1994;15:505–513. [PubMed: 7980961]
65. Phelps JB, Hubbard GB, Wang X, Agrawal CM. Microstructural heterogeneity and the fracture toughness of bone. J Biomed Mater Res 2000;51:735–41. [PubMed: 10880123]
66. McKee MD, Addison WN, Kaartinen MT. Hierarchies of extracellular matrix and mineral organization in bone of the craniofacial complex and skeleton. Cells Tissues Organs 2005;181:176–88. [PubMed: 16612083]
67. McKee, MD.; Kaartinen, MT. Regulation of biomineralization by bone proteins and their assembly into extracellular matrices: implications for implant osseointegration. In: Zarb, G.; Lekholm, U.; Albrektsson, T.; Tenenbaum, H., editors. Aging, Osteoporosis and Dental Implants. Caro Stream: Quintessence Pub. Co. Inc.; 2002. p. 191-206.
68. Kohn DH, Sahar ND, Wallace JM, Golcuk K, Morris MD. Exercise alters mineral and matrix composition in the absence of adding new bone. Cells Tissues Organs 2009;189:33–7. [PubMed: 18703871]
69. Wallace JM, Ron MS, Kohn DH. Short-term exercise in mice increases tibial post-yield mechanical properties while two weeks of latency following exercise increases tissue-level strength. Calcif Tissue Int 2009;84:297–304. [PubMed: 19283427]
70. Ionova-Martin SS, Do SH, Barth HD, Szadkowska M, Porter AE, Ager JW 3rd, Ager JW Jr, Alliston T, Vaisse C, Ritchie RO. Reduced size-independent mechanical properties of cortical bone in high-fat diet-induced obesity. Bone. 2009
71. Peterlik H, Roschger P, Klaushofer K, Fratzl P. From brittle to ductile fracture of bone. Nat Mater 2006;5:52–5. [PubMed: 16341218]
72. Gupta HS, Seto J, Wagermaier W, Zaslansky P, Boesecke P, Fratzl P. Cooperative deformation of mineral and collagen in bone at the nanoscale. Proc Natl Acad Sci U S A 2006;103:17741–6. [PubMed: 17095608]
73. Stolz M, Gottardi R, Raiteri R, Miot S, Martin I, Imer R, Staufer U, Raducanu A, Duggelin M, Baschong W, Daniels AU, Friederich NF, Aszodi A, Aebi U. Early detection of aging cartilage and osteoarthritis in mice and patient samples using atomic force microscopy. Nat Nanotechnol 2009;4:186–92. [PubMed: 19265849]
74. Noda M, Yoon K, Prince CW, Butler WT, Rodan GA. Transcriptional regulation of osteopontin production in rat osteosarcoma cells by type beta transforming growth factor. J Biol Chem 1988;263:13916–21. [PubMed: 3166460]

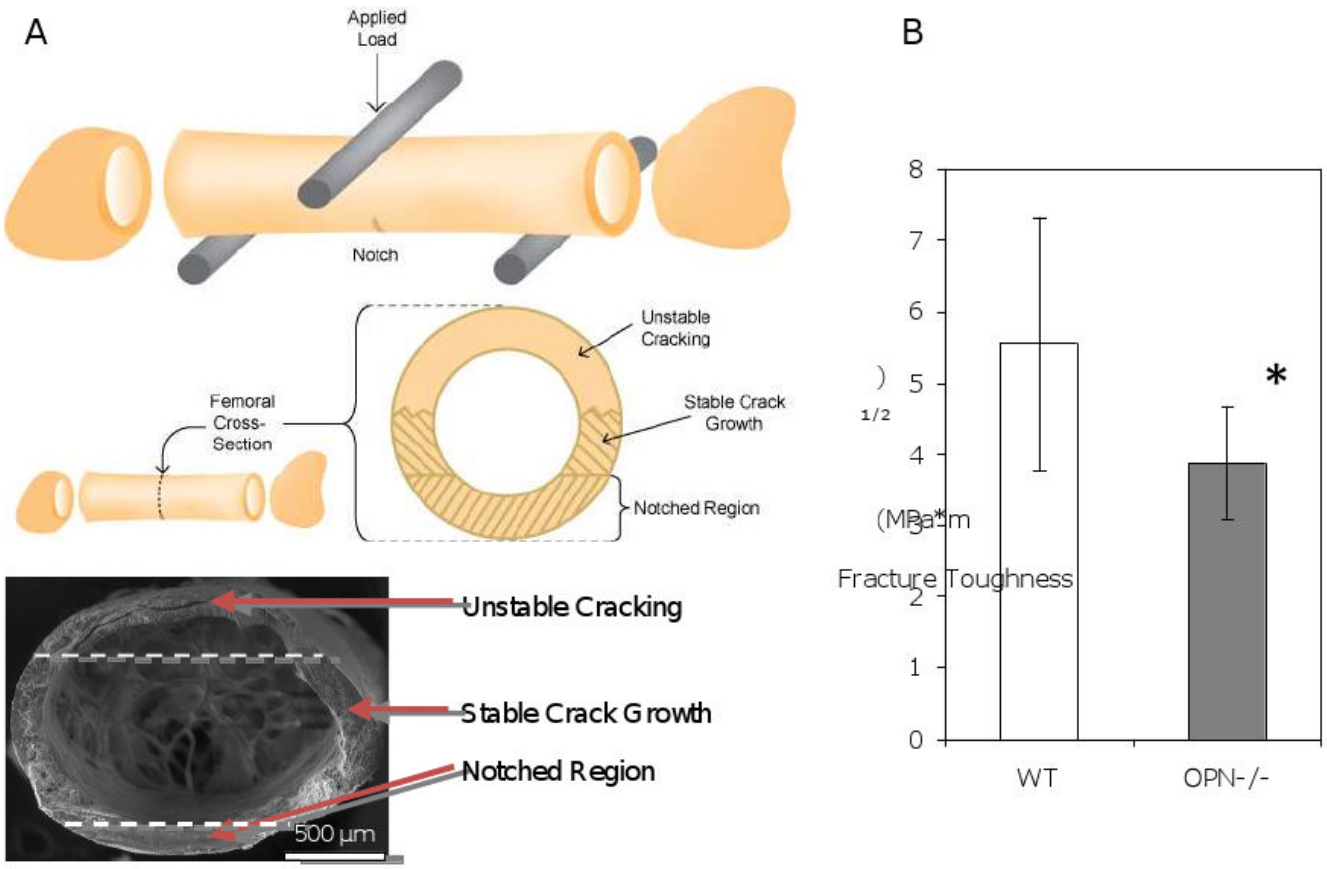

Figure 1. OPN-deficient bone has reduced fracture toughness

The test configuration is shown schematically (A). A notched femur is tested in three-point bending, with the polished notch on the posterior of the femur, opposite the applied load. An examination of the broken cross section (bottom of schematic and SEM image) after the test reveals a smooth notched region, from which extends a stable crack growth region, followed by unstable cracking for the remaining circumference of the sample (approximate borders between these regions are indicated with dashed lines in the SEM image). Further details on this fracture toughness testing procedure are described in [43]. Asterisks (*) indicate statistically significant differences in fracture toughness ($p<0.05$) in WT and OPN-deficient bone. (B).

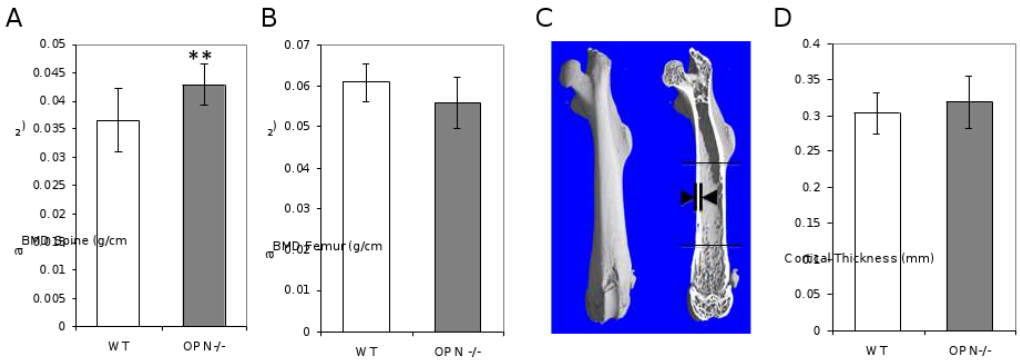

Figure 2. Femoral bone mineral density and cortical thickness are not affected by OPN deficiency

DEXA analysis of dissected spines (A), but not femora (B), showed OPN-dependent differences in areal bone mineral density (aBMD), (**, $p<0.01$). As shown by the arrows in panel C, micro-computed tomography data of dissected femora from OPN-/- mice and their wild-type littermates were used to determine cortical thickness (D).

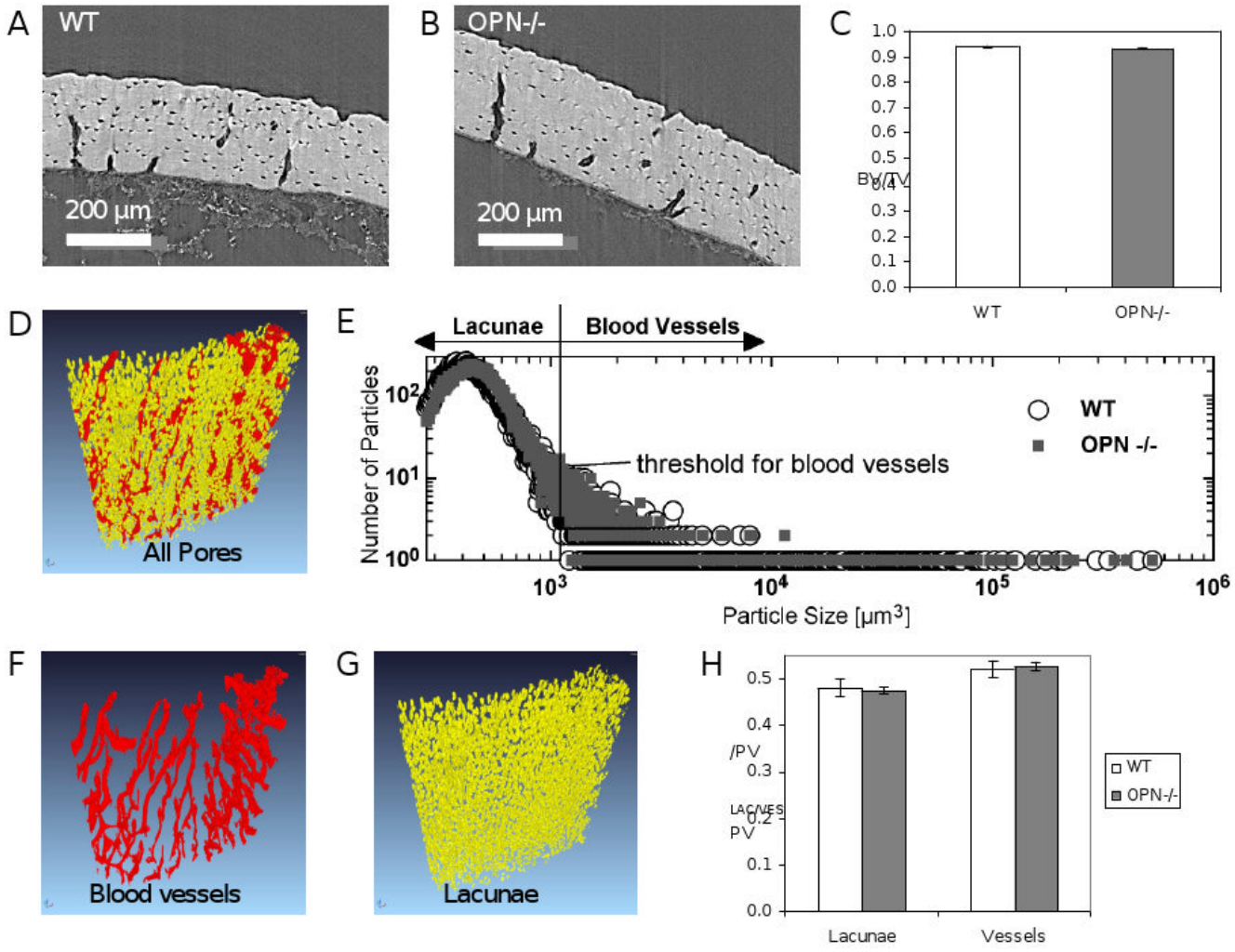

Figure 3. Cortical bone porosity is not affected by OPN-deficiency

Synchrotron radiation micro-computed tomographic (SRµCT) analysis of cortical femoral bone from OPN-/- mice (B) and wild-type littermates (A) showed no differences in bone volume (BV/TV) (C). The size distribution of cortical bone pores was assessed in wild-type (open circles) and OPN-/- mice (grey squares) using reconstructed images (D, E). Based on particle size, pores were segmented as blood vessels (F) or osteocyte lacunae (G). Quantitative analysis of lacunar pore volume (PV_{Lac}/PV) and blood vessel volume (PV_{Ves}/PV) showed no OPN-dependent differences (H).

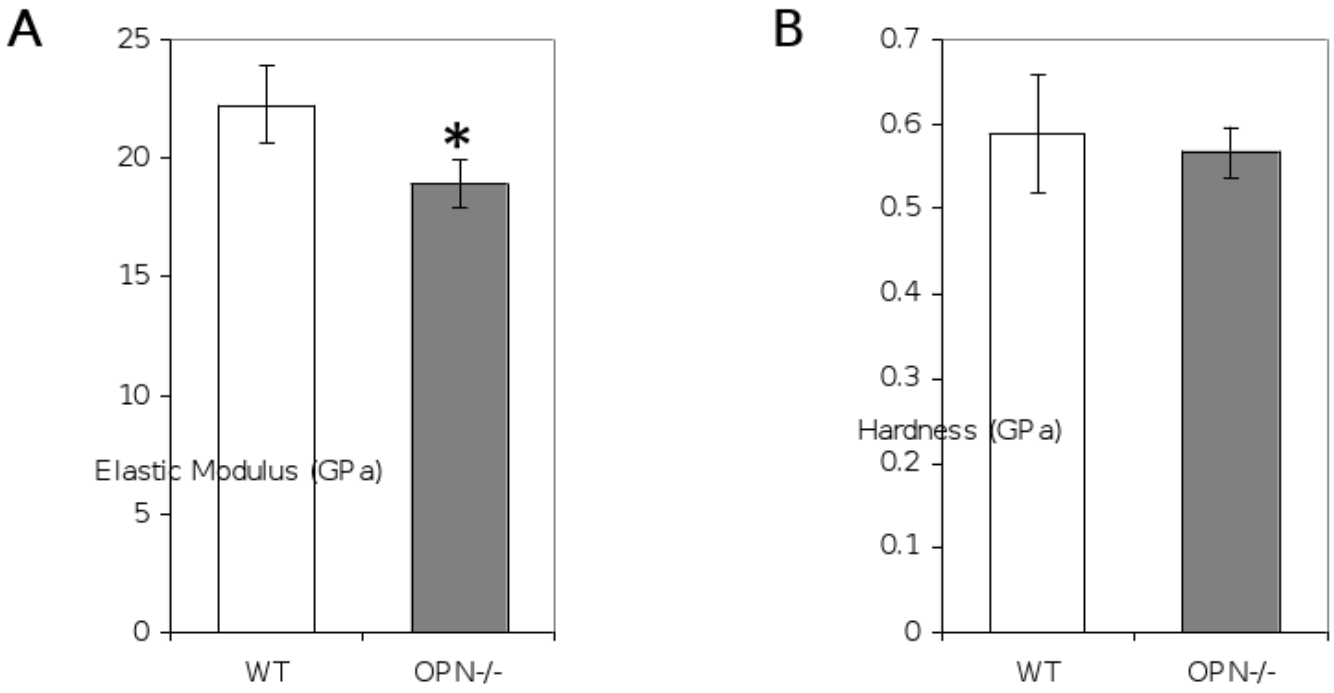

Figure 4. OPN-deficiency impairs the elastic modulus of cortical bone matrix

Cross-sections of polished mid-tibial cortical bone matrix were assessed by nanoindentation to determine elastic modulus (A) and hardness (B), (*, $p<0.05$).

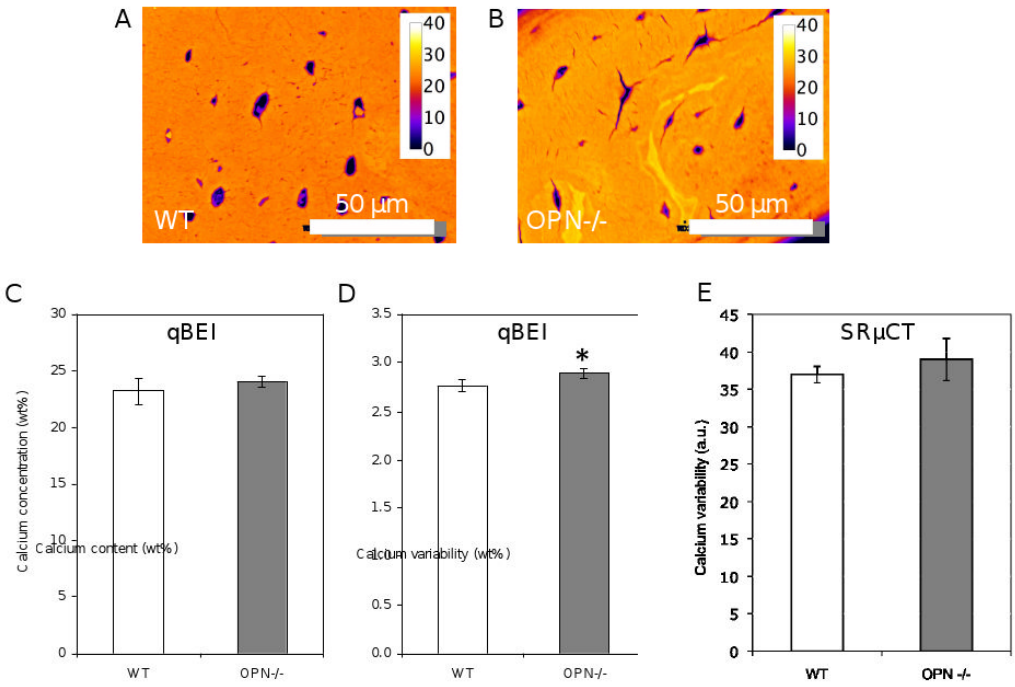

Figure 5. OPN-deficiency increases mineral heterogeneity

Bone specimens equivalent to those in Figure 4 were assessed by quantitative backscattered electron imaging to evaluate local variation in matrix mineralization in wild-type (A) and OPN-/- (B) mice. Mineral concnetration in bones was calibrated to standards to produce a pseudo-color scale, with yellow regions indicating the highest mineral concentration (given in wt%). Though no differences in mineral concentration were detected (C), OPN-/- bone matrix had significantly increased mineral heterogeneity (D), (*, $p<0.05$). A similar, however, insignificant trend in mineral heterogeneity was also detected in the samples imaged with synchrotron radiation micro-computed tomography (SRµCT) (E).

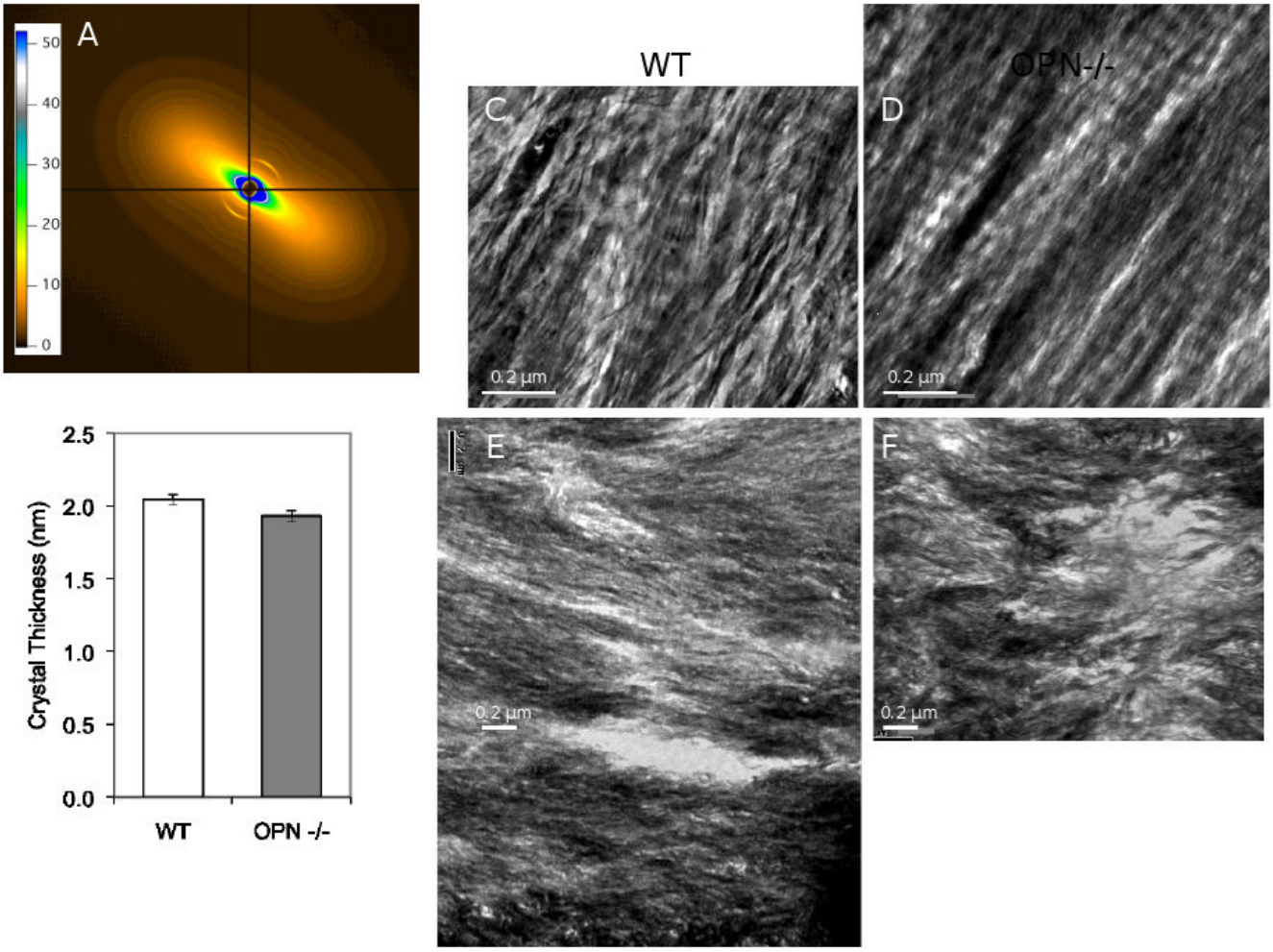

Figure 6. Analysis of mineral and collagen size and organization

Panel A shows a representative diffraction pattern from small angle X-ray scattering analysis, which showed trends (p=0.09) towards lower crystal thickness in OPN-deficient (1.930 ± 0.039) nm vs. WT (2.044 ± 0.036) nm tibial cortical bone (B). Representative images of samples prepared by focused ion beam (FIB) milling (C, D) showed no differences in collagen organization; but those prepared by ultramicrotomy showed increased in matrix disorganization in OPN-/- femoral cortical bone matrix (F) relative to wild-type (E).

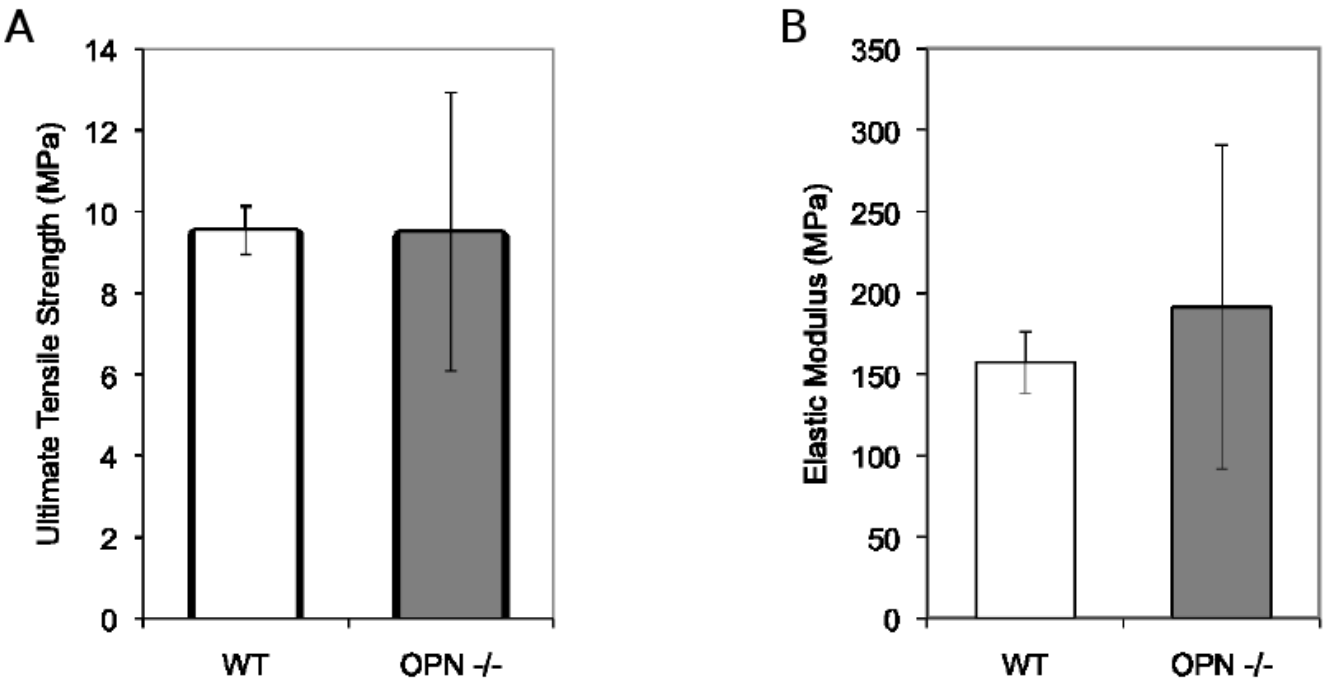

Figure 7. OPN-deficiency does not compromise the tensile strength of demineralized bone matrix
Tensile testing of specimens of demineralized femoral bones showed no difference in tensile strength (A) or elastic modulus (B).

Table 1

Quantitative analysis of apatite and collagen by transmission electron microscopy.

Variable	Wild-type	OPN-deficient
Apatite Thickness (nm)	2.26 ± 0.38	2.16 ± 0.48
Collagen Fibril Width (nm)	79.14 ± 2.20	78.8 ± 2.33
Collagen Banding (nm)	67.3 ± 2.42	65.1 ± 2.67